A PHOTOELASTIC TECHNIQUE FOR THE DETERMINATION OF STRESS INTENSITY FACTORS FOR MODE III LOADING

by

William Thor Hardrath

Thesis submitted to the Graduate Faculty of the
Virginia Polytechnic Institute and State University
in partial fulfillment of the requirements for the degree of
MASTER OF SCIENCE
in
Engineering Mechanics

APPROVED:

C. W. Smith, Chairman

W. W. Stinchcomb

K. L. Reifsnyder

August, 1978

Blacksburg, Virginia

ACKNOWLEDGEMENTS

The author wishes to express his deepest gratitude to

for his suggestions, encouragement, and friendship extended over the years. Thanks are also due to Professors

and for their contributions of time and effort.

The suggestions and assistance of

and are also appreciated.

The support of this work by the National Science Foundation under Grant No. is gratefully acknowledged.

TABLE OF CONTENTS

LIST OF FIGURES

LIST OF TABLES

NOTATION

a - crack depth

b - maximum radius of test specimen

c - radius to notch front

E - modulus of elasticity

f - material fringe value

J - polar moment of inertia

K - stress intensity factor

K_{AP} - apparent stress intensity factor

n,t,z - local crack tip coordinates

n' - stress fringe order

r,θ - crack tip polar coordinates

$\overline{r}$ - integrated average distance from crack tip

t' - slice thickness

β - angle of rotation of the analyzer when applying the Tardy method

ν - Poisson's ratio

ρ - notch root radius

σ - normal stress component

σ°, τ° - regular stress field terms in crack tip stress equations

τ - shear stress component

$\overline{\tau}$ - nominal stress at notch root

I. INTRODUCTION

The use of high strength alloys in the fabrication of structures for applications such as bridges, pipelines, pressure vessels, and aerospace vehicles is becoming increasingly common. That these alloys are often brittle and sensitive to the presence of flaws necessitates fracture mechanics analyses of the structures, particularly when the structure will be subjected to repeated loading cycles.

Structures are often subjected to complex loading conditions which may not be symmetric, and flaws will probably not be oriented in any specific fashion with respect to the loads. These factors make the use of mixed mode fracture mechanics analyses desirable.

In the past, most fracture mechanics research, both experimental and analytical, has been carried out for two dimensional models and Mode I or crack opening displacements. Relatively few three dimensional problems have been solved in closed form [1,2,3] and these have been infinite body problems. More often, problems of this type are solved using numerical techniques and digital computers and considerable progress has been made in this fashion [4,5]. However, rigorous convergence proofs are usually not available, making independent computer code verification necessary.

To avoid some of the difficulties noted above, C. W. Smith and his associates, beginning with an idea of G. R. Irwin's [6], developed an experimental technique for estimating stress intensity factors from photoelastic data [7-20]. This method was originally applied solely

to Mode I problems, but was later extended to include mixed Mode I and Mode II loadings [9,20].

Recently, in attempting to analyze surface flaws under mixed mode loadings, attempts to measure K_{III}, the Mode III stress intensity factor, proved unsuccessful [20]. This failure may have been due to relatively small Mode III effects. As a result, the present study was undertaken to determine the feasibility of measuring K_{III} photoelastically. To accomplish this, a loading condition and geometry yielding pure Mode III displacements and for which analytical or numerical results were available for comparison were required. A torsionally loaded, circumferentially notched circular cylinder was chosen.

In this thesis the method for extracting Mode III stress intensity factors from the photoelastic data will be developed. The results of the experimental program will be compared with analytical and numerical results drawn from the literature.

II. ANALYTICAL BACKGROUND FOR THE MODE III PROBLEM

Based upon Inglis' [21] work for an elliptical hole in an infinite plate under uniaxial tension, Griffith [22], in 1920, published his concept of crack propagation stating that a crack will propagate if the total energy of the system is reduced thereby. The concept of a stress intensity factor was first presented by Irwin [23] in his development of equations for stresses and displacements in the vicinity of a crack tip. He demonstrated that his equations relating the stress intensity factor to stresses and strains were equivalent to the earlier work by Griffith based on energy release. The stress intensity factor, as postulated by Irwin, is related to applied loads and problem geometry and controls the level of stresses around a crack tip but not the distribution.

Kassir and Sih [24] showed that, for an arbitrarily loaded elliptical crack, the stresses near the crack tip could be represented by a functional relation similar to that proposed by Irwin for the Mode I case if a set of moving, local coordinate axes was used. These local coordinates (n,z,t) are oriented such that the z axis is perpendicular to the plane of the crack, n is perpendicular to the flaw border in the plane of the crack, and t is located tangent to the flaw border in the crack plane (Fig. 2.1). The stress components can be written as:

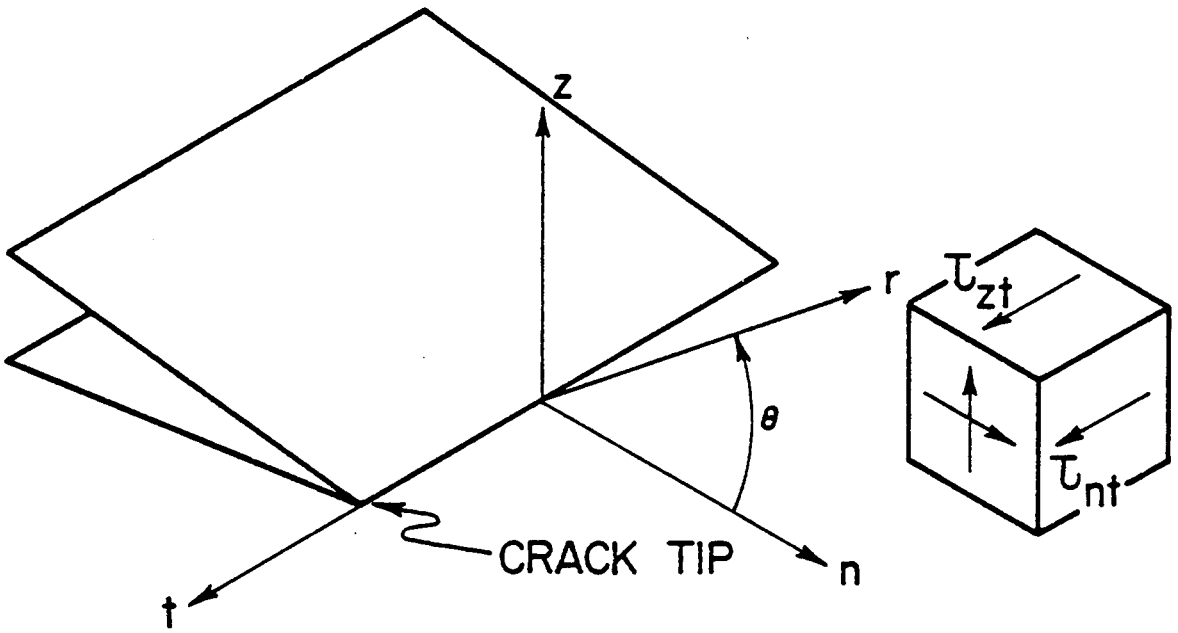

Figure 2.1 Crack Tip Stress Notation for the Mode III Problem

$$\sigma_{nn} = \frac{K_I}{(2\pi r)^{1/2}} \cos\frac{\theta}{2}\left(1 - \sin\frac{\theta}{2}\sin\frac{3\theta}{2}\right)$$

$$- \frac{K_{II}}{(2\pi r)^{1/2}} \sin\frac{\theta}{2}\left(2 + \cos\frac{\theta}{2}\cos\frac{3\theta}{2}\right) - \sigma^{\circ}_{nn}(r,\theta)$$

$$\sigma_{zz} = \frac{K_I}{(2\pi r)^{1/2}} \cos\frac{\theta}{2}\left(1 + \sin\frac{\theta}{2}\sin\frac{3\theta}{2}\right)$$

$$+ \frac{K_{II}}{(2\pi r)^{1/2}} \sin\frac{\theta}{2}\cos\frac{\theta}{2}\cos\frac{3\theta}{2} - {}^{\circ}_{zz}(r,\theta)$$

$$\sigma_{tt} = \frac{K_I}{(2\pi r)^{1/2}} 2\nu \cos\frac{\theta}{2} - \frac{K_{II}}{(2\pi r)^{1/2}} 2\nu \sin\frac{\theta}{2} - \sigma^{\circ}_{tt}(r,\theta) \quad (2.1)$$

$$\tau_{nz} = \frac{K_I}{(2\pi r)^{1/2}} \sin\frac{\theta}{2}\cos\frac{\theta}{2}\cos\frac{3\theta}{2}$$

$$+ \frac{K_{II}}{(2\pi r)^{1/2}} \cos\frac{\theta}{2}\left(1 - \sin\frac{\theta}{2}\sin\frac{3\theta}{2}\right) - \tau^{\circ}_{nz}(r,\theta)$$

$$\tau_{nt} = - \frac{K_{III}}{(2\pi r)^{1/2}} \sin\frac{\theta}{2} - \tau^{\circ}_{nt}(r,\theta)$$

$$\tau_{zt} = \frac{K_{III}}{(2\pi r)^{1/2}} \cos\frac{\theta}{2} - \tau^{\circ}_{zt}(r,\theta)$$

where the notation is described in Figure 2.1, K_I, K_{II} and K_{III} are the stress intensity factors associated with Mode I, Mode II and Mode III displacements respectively and the σ°_{ij} are the contributions of the regular stress field. The σ°_{ij} will generally vary along the crack front but will be constant for a single point on the crack front.

It will be noted that only the last two of Equations 2.1 contain K_{III}, the Mode III stress intensity factor. Thus, for pure Mode III loading, the shear stresses τ_{nt} and τ_{zt} will be the only non-zero stress components, and will be equal to the maximum shear stresses in their respective planes. If Mode I or Mode II loading is present, this will not be true and τ_{max} will be a function of the stress intensity factors corresponding to the loading modes present. However, K_I and K_{II} may be solved for independently of K_{III} [20], allowing the extraction of a value for K_{III}.

For the work presented in this thesis, both K_I and K_{II} are zero resulting in a great simplification of the equations. The maximum shear stresses present in the z-t and n-t planes will be τ_{zt} and τ_{nt} respectively. If only planes intersecting the crack tip are considered, the angle θ will be zero for the n-t plane and $\pi/2$ for the z-t plane. The equations for τ_{nt} and τ_{zt} thus reduce to:

$$\begin{aligned} \tau_{nt} &= -\tau^{\circ}_{nt} \\ \tau_{zt} &= \frac{K_{III}}{(4\pi r)^{1/2}} - \tau^{\circ}_{zt} \end{aligned} \tag{2.2}$$

τ_{nt} will not be dependent on K_{III} and may be ignored for the present. τ_{zt} will be the component from which K_{III} is extracted.

If a new quantity, known as the apparent stress intensity factor, is defined as:

$$K_{AP} = \tau_{max}(4\pi r)^{1/2} , \tag{2.3}$$

Equation 2.2 for the z-t plane may be rewritten as:

$$K_{AP} = K_{III} - \tau^{\circ}_{zt}(4\pi r)^{1/2} \tag{2.4}$$

It is often convenient to present values of stress intensity factors in normalized form. The above equation may be divided by a normalizing factor of $\bar{\tau}(\pi a)^{1/2}$ where $\bar{\tau}$ is a parameter defining the remote stress state and a is the crack depth. The normalized form of Equation 2.4 is:

$$\frac{K_{AP}}{\bar{\tau}(\pi a)^{1/2}} = \frac{K_{III}}{\bar{\tau}(\pi a)^{1/2}} - \frac{2\tau^{\circ}_{zt}}{\bar{\tau}}\left(\frac{r}{a}\right)^{1/2} \tag{2.5}$$

This equation, when plotted as $\frac{K_{AP}}{\bar{\tau}(\pi a)^{1/2}}$ vs. $\left(\frac{r}{a}\right)^{1/2}$, yields a straight line which if extrapolated to $\left(\frac{r}{a}\right)^{1/2} = 0$ will yield $\frac{K_{III}}{\bar{\tau}(\pi a)^{1/2}}$, the normalized Mode III stress intensity factor.

It has been shown how K_{III} may be obtained if the distribution of τ_{zt} along a line perpendicular to the crack plane and passing through the crack front is known. The primary value obtained from a photoelastic analysis is the maximum shear stress in a plane perpendicular to the direction of light transmission. If a slice is taken from a photoelastic model which has been put through a stress freezing cycle (the details of this procedure will be covered in the following section), the distribution of τ_{max} can be determined. At any point on the slice, the maximum shear stress will be given by:

$$\tau_{max} = \frac{n'f}{2t'} \tag{2.6}$$

where n' is the fringe number, f is the material fringe value, and t' is the thickness at that point. Thus, it may be seen, that by taking a slice in the z-t plane centered on the crack tip, the necessary distribution of τ_{max} may be obtained.

III. EXPERIMENTAL BACKGROUND AND PROCEDURE

The technique of stress freezing photoelasticity dates from the work of Oppel [30] and makes use of the diphase properties of certain transparent materials to obtain data on the stresses in three dimensional problems. The materials used for stress freezing models exhibit viscoelastic response to mechanical loads at room temperature. That is, mechanical loads will cause optical and mechanical creep or flow in addition to elastic deformation. However, above the so-called critical temperature, the viscous material constant approaches zero and the material then behaves in a linear elastic and time independent fashion with an elastic modulus approximately two orders of magnitude lower and an isochromatic fringe sensitivity about twenty-five times greater than the values at room temperature. If the material is heated above critical, loaded, and allowed to cool under load, the recovery is negligible due to the change in elastic modulus and isochromatic fringe sensitivity. The deformation and isochromatic fringe evidence of the live loads applied above critical temperature are thus "frozen" into the material. No macrostresses are retained in the model making the term "stress freezing" somewhat of a misnomer. However, the lack of stress permits the model to be sectioned and the stresses resulting from the applied load determined in any plane by examining slices in a crossed circular polariscope.

The photoelastic method is presented in detail in references such as [31,32] and so the subject will not be dwelt upon at great length

in this thesis. However, a brief discussion of the principles applicable to the current problem and procedures used is desirable.

There are a number of transparent materials which become double refracting upon the application of load. That is, if a ray of light enters the material along one of the principal stress directions, it will be divided into two components having planes of polarization parallel to the planes of principal stress. Each component will travel through the material at a different speed, which depends on the magnitudes of the principal stresses. This effect is normally present only so long as the loads on the body are maintained but may be retained permanently by the stress freezing procedure.

If the double refracting material is placed in a crossed circular polariscope, an interference pattern will be observed. If monochromatic light is used, the pattern will consist of light and dark bands known as isochromatic or stress fringes. The dark fringes are assigned integral fringe orders n', beginning at n' = 0, proportional to the maximum in-plane shear stress by the relation given in Equation 2.6. The use of white light will cause the interference pattern to appear as a spectrum of colors. The border between the red and blue fringes is located at the same point as the center of the dark fringe observed using monochromatic light.

If the number of fringes is not adequate for the accurate determination of the linear zone used in the estimation of the stress intensity factor, the number of data points taken may be increased by measuring fractional fringe orders. In this case the Tardy method is applied. To do so, a plane polariscope is first used to locate the

planes of principal stress at the locations at which data are desired. The circular polariscope is then oriented with its polarizing axes parallel to the principal stress planes. Now, if the second polarizing plate (the analyzer) is rotated an angle β from its initial position, the fringe orders will shift by the quantity $\beta/180$. Thus, the application of this technique allows data to be taken at many more points than would be possible if only the integral fringe orders were used.

This introduction to the photoelastic method and the stress freezing procedure as they apply to the current problem will simplify descriptions of the procedures in the following portion of this chapter. It will also give some insight into the reasons for choosing certain of these procedures.

In order to insure adequate Mode III field strengths and simultaneously provide analytical solutions [25,26,27,28] for comparison, the test geometry selected was an external circumferential crack in a circular shaft under torsional loading. For this series of tests, sharp 30° vee notches were machined around the circumference of 52-mm diameter circular cylinders of PLM-4B (Figure 3.1), a stress freezing photoelastic material manufactured by Photolastic, Inc. The machined notches were chosen over natural cracks to allow close control of the problem geometry. Notches of the geometry chosen have been shown analytically [29] and experimentally [16] to behave in a manner similar to natural cracks for Mode I loading and so were expected to yield satisfactory results. After machining, the specimens were suspended in an oven, heated above critical, loaded by dead weight through steel pins and a fork arrangement (Figure 3.2), and slowly cooled, freezing

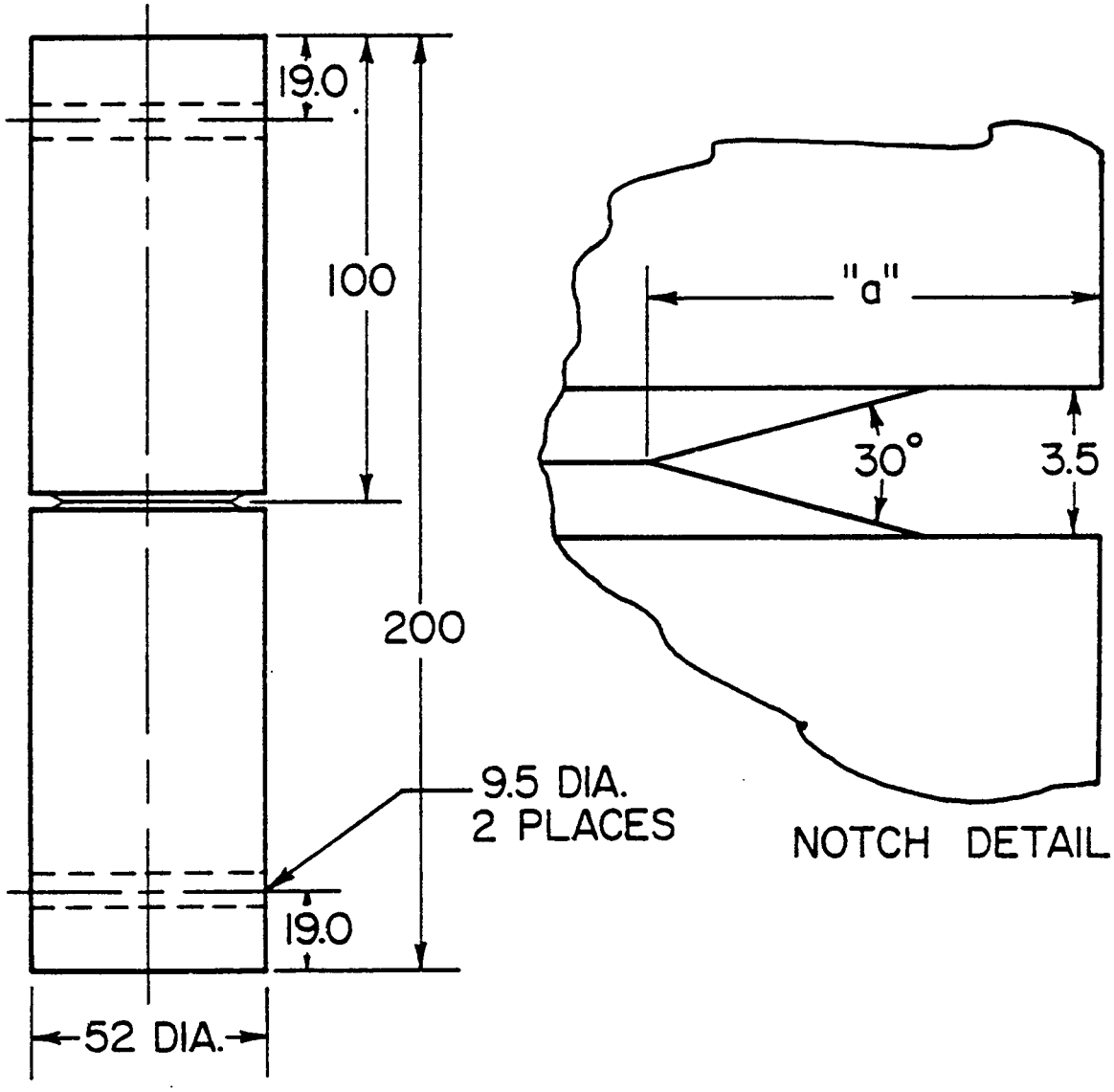

Figure 3.1 Geometry of Test Specimen

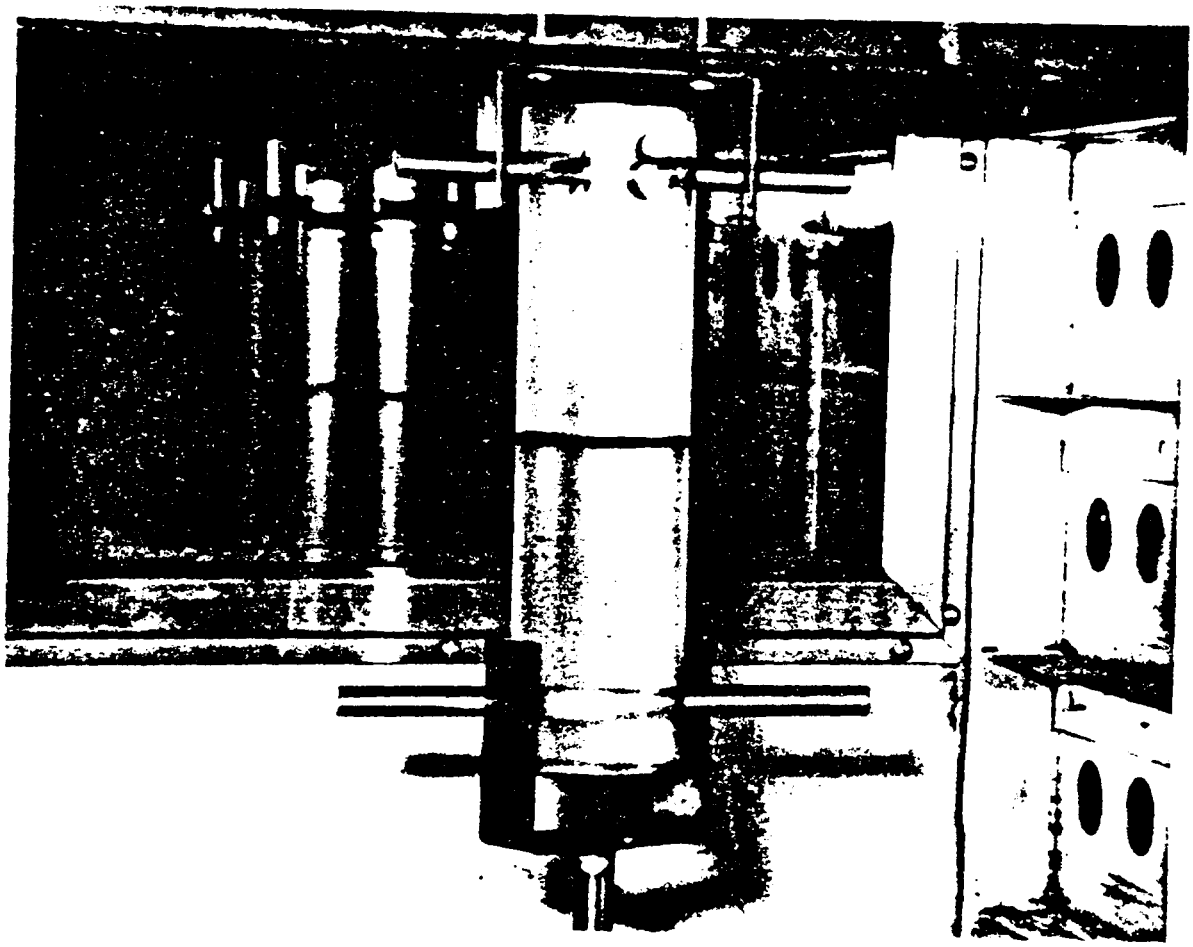

Figure 3.2 Test Specimen and Loading Rig Mounted in the Stress Freezing Oven

in the deformations and fringes.

Upon completion of the stress freezing cycle, the model was removed from the oven and sliced. Three types of slices were taken from each model. Surface slices were cut from the regions far from the load points and the notch and used to determine the material fringe value. Slices were cut in the n-z plane (perpendicular to the notch plane and the notch front) for the determination of notch depth; the presence of any Mode I or Mode II loading could also be ascertained. Finally, slices in the z-t plane (perpendicular to the notch plane and tangent to the notch front), centered on the notch tip were cut (Figure 3.3). From the last slices, the data used for the determination of stress intensity were taken. The slices were cut from the model using either a vertical band saw or a hand-held jeweler's saw and the cut surfaces smoothed by sanding.

The material fringe value is determined from the surface slices in the following manner. The slice is coated with an oil having the same index of retraction as the model material and placed in a crossed circular polariscope. A full field null balance compensator is used to determine the absolute fringe order on the line along which the slice is tangent to the cylinder surface. This value will be related to the average shear stress in the slice along the same line (Equation 2.6). The average shear stress is then calculated from the relation

$$\tau_{av} = \frac{T}{J}\left(\frac{2b - t'}{2}\right) \tag{3.1}$$

where T is the applied torque, J is the polar moment of inertia of the cylinder, b is the outside radius, and t' is the thickness of the

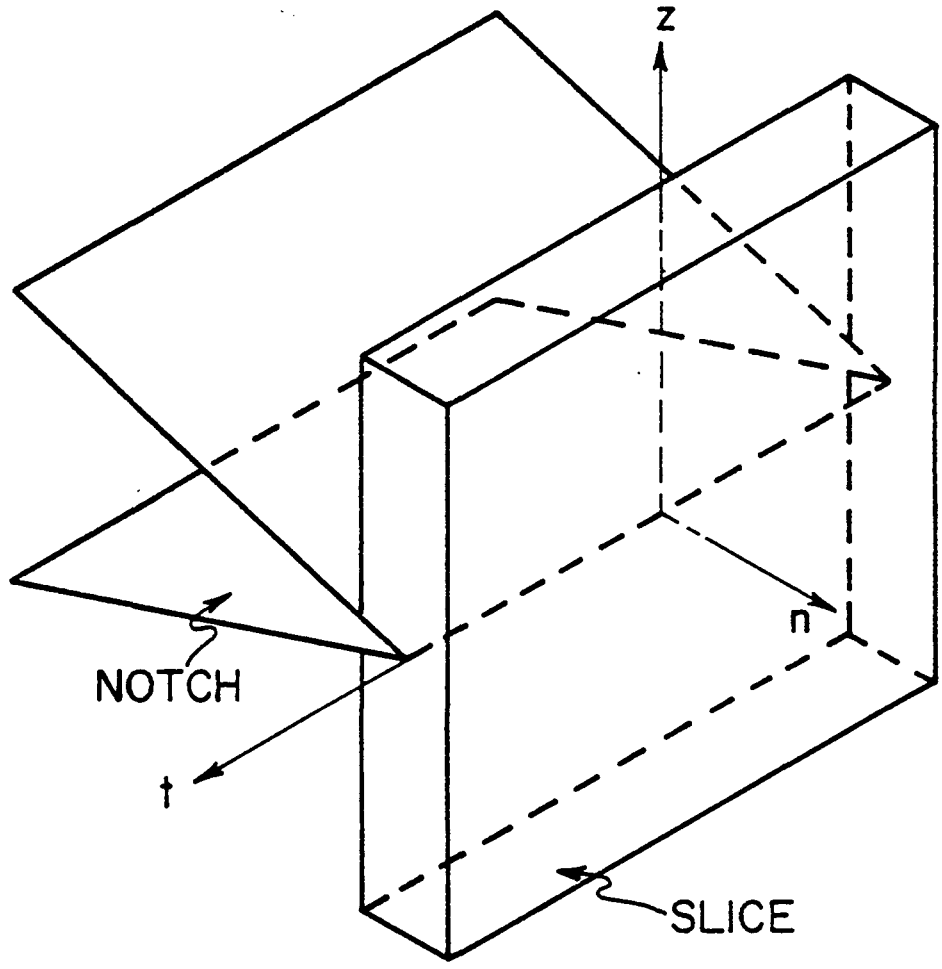

Figure 3.3 Slice Location for the Determination of τ_{zt}

slice. By equating 2.6 and 3.1, and solving for f, the following relation is obtained:

$$f = \frac{Tt'}{Jn'} (2b - t') \tag{3.2}$$

and the calibration of the material is thus accomplished.

The slices cut perpendicular to the notch plane and the notch front are also coated with oil and examined in the polariscope for the presence of Mode I fringes; none have been found in the course of this work. At the same time the notch depth is measured using the micrometer stage of the polariscope.

Having thus obtained values for the constants used in the determination of the stress intensity factor, the isochromatic fringes in the slices cut tangent to the notch tip are examined and data obtained for the calculation of stress intensity factor as outlined in the previous chapter. The procedure used is as follows. The slice is, again, coated with oil and viewed in a plane polariscope and the directions of the principal planes of stress determined in the direction of fringe spreading ($\theta = \frac{\pi}{2}$ for the work described herein). The elements of the circular polariscope are then oriented for the application of the Tardy method as described previously.

When placed in the polariscope a fringe pattern such as the one shown in Figure 3.4 is generated. The data required for the calculation of stress intensity factors from Equations 2.3, 2.5, and 2.6 consists of the order, n', of a given fringe and its distance, r, from the notch tip. Usually, data are taken starting with the lowest fringe order. The fringe order is recorded and its distance from the

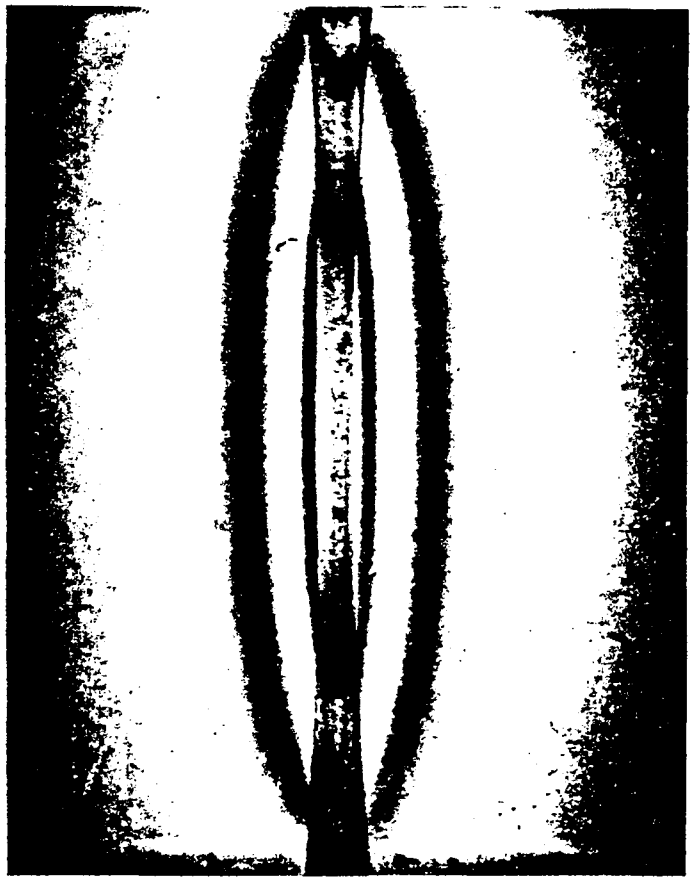

Figure 3.4 Typical Fringe Pattern

notch tip measured and recorded. Then the analyzer is rotated until the fringe order is increased by 0.1. The distance from the notch tip is again measured and recorded. This procedure is repeated until the intersection of the notch surface with the slice surface is reached, beyond which point meaningful data are impossible to obtain due to the rapid variation in thickness. Following this procedure, data have generally been taken over to 1-1/2 fringe orders.

From the data thus recorded, the normalized apparent stress intensity factor is calculated from Equations 2.3 and 2.6. This value and the corresponding value of the square root of the normalized distance from the crack tip are then used to construct a graph such as the one shown in Figure 3.5. A least squares analysis is used to construct a straight line through the linear part of the data. This straight line is then extrapolated to $\left(\frac{r}{a}\right)^{1/2} = 0$ to obtain the normalized stress intensity factor. Data taken at small values of $\left(\frac{r}{a}\right)^{1/2}$ (less than about 0.2) may not fall along the extrapolated straight line. This behavior is observed for all loading conditions and geometries and is thought to be caused by crack tip blunting and a variation of constraint as the crack tip is approached. The results outside of the non-linear zone are not affected and so these points are disregarded.

Four slices can easily be obtained from each test specimen, thus yielding four separate values of K_{III} for each test. The average value of K_{III} is calculated for each geometry and used for comparison with other solutions.

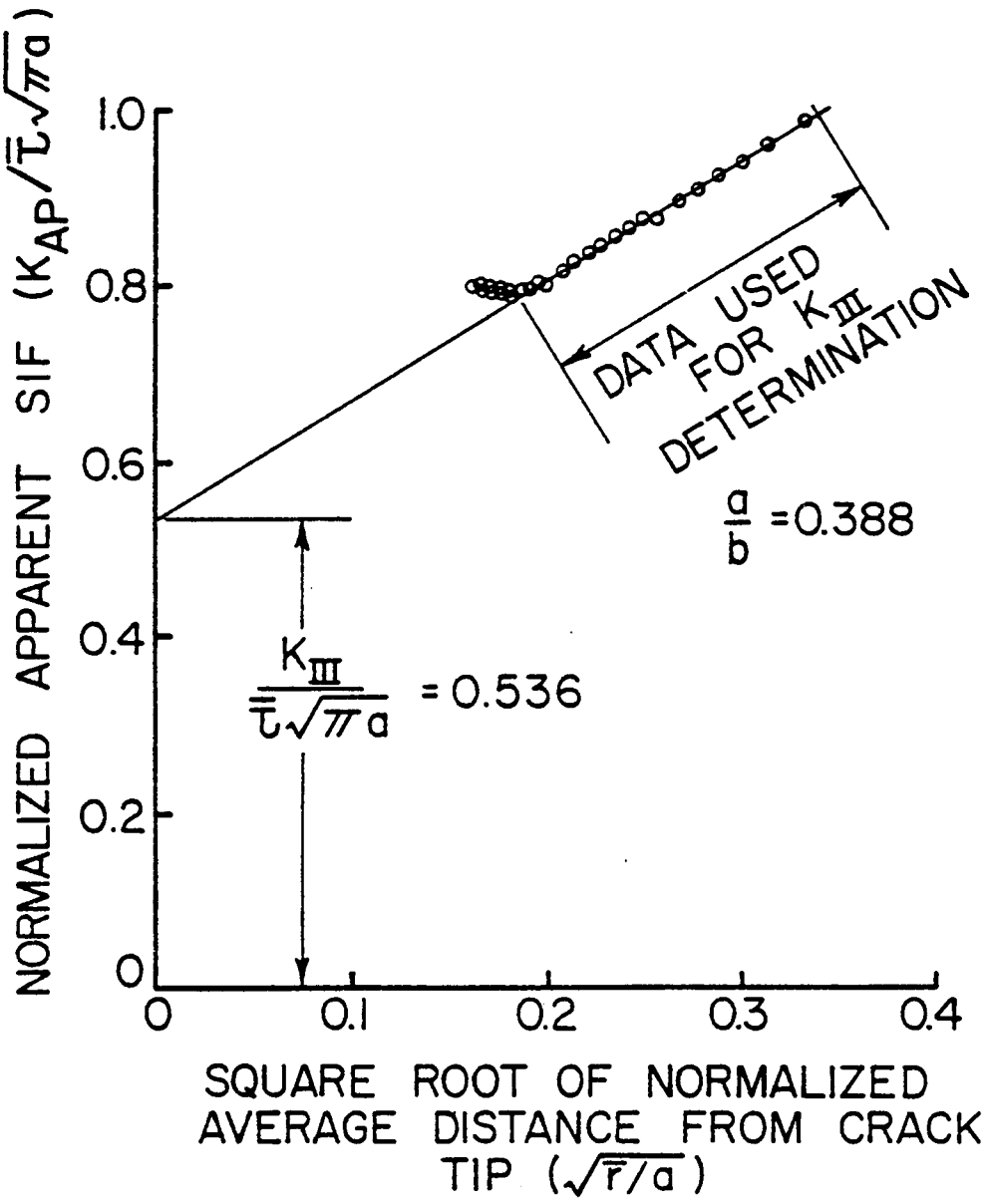

Figure 3.5 Typical Data Set

IV. RESULTS AND DISCUSSION

The problem of a torsionally loaded, circumferentially notched round shaft has been solved analytically by Harris [25], and Benthem and Koiter [26]. The problem was also examined by Wilson [27], and Yamamoto and Sumi [28] using a finite element method. Harris utilized the work of Neuber on stress concentration factors at notches to solve for stress intensity factors in hollow circumferentially notched round bars loaded in axial tension, bending, and torsion. The solutions for tensile and bending loads were verified experimentally. Wilson compared his results using the finite element method with those of Harris for the case of torsional loading and found the two sets to be within 5% of each other. Benthem and Koiter employed an asymptotic approximation for the problem of a circular cylinder containing either a penny-shaped internal crack or a ring-shaped external crack loaded in a variety of ways. Upon examination, their results are found to be close to Harris' and to agree very closely with Wilson's. Yamamoto and Sumi obtained results which are almost identical to those of Benthem and Koiter.

The consistency of the published analytical and numerical solutions suggests that the results are close to the true value of SIF for the problem. In addition, since Harris' work was for sharp notches while Wilson, Benthem and Koiter, and Yamamoto and Sumi used plane cracks, the sensitivity of the problem to notch geometry can be determined.

The experimental results are presented in Table 4.1 and Figure 4.1 and are compared with the analytical and numerical results discussed previously. The agreement between the experimental and analytical results is quite good although the experimental values are slightly higher than the analytical. However, in all except one case the difference between the experimentally determined values of K_{III} and the solution by Benthem and Koiter is less than 5%. The point at $\frac{a}{b} = .09$ is about 9% higher than the analytical solution. However, this point is the average of significantly different results from only two slices. This point is the most uncertain of all of the results.

In the course of this work, slice thickness was found to have a considerable effect on the results if calculations were made using the measured value of r. After obtaining a few anomalous values of stress intensity factor, it was decided to assess the effect of slice thickness. A number of slices were sanded progressively thinner and data taken at each thickness. When the results are compared, it is observed that the stress intensity factor estimate is higher for thinner slices (Figure 4.2). The experimentally determined values may approach the solution by Benthem and Koiter as the slices approach zero thickness. However, reduction of slice thickness below about .5 mm is difficult with the present sanding technique. Furthermore, data scatter becomes more pronounced and the results less certain as the slice thickness is reduced. This is due to several factors, among which are: small thickness variations become a larger percentage of total thickness, data are taken over fewer fringes, and the fringes are less sharp.

Table 4.1

EXPERIMENTAL RESULTS

Specimen	a/b	Slice	Thickness (mm)	$K_{III}/\bar{\tau}(\pi a)^{1/2}$	Mean	Standard Deviation
1	.090	5	1.04	.965	.901	.091
		6	1.22	.836		
2	.099	1	1.24	.760	.811	.051
		2	0.66	.821		
			0.76	.827		
			1.02	.896		
		3	0.64	.806		
			0.76	.772		
			1.02	.758		
			1.27	.779		
		4	1.27	.884		
3	.334	1	1.37	.572	.532	.039
			1.96	.561		
		2	0.74	.509		
			0.99	.506		
			1.24	.509		
			1.50	.506		
		3	1.35	.521		
			1.50	.498		
		4	1.50	.609		
6	.148	1	1.50	.761	.775	.042
		2	1.50	.755		
		3	1.50	.743		
			1.50	.766		
		4	1.52	.849		
8	.388	1	1.47	.493	.479	.054
		2	1.35	.532		
		3	0.51	.475		
			0.91	.403		
			1.42	.431		
		4	1.02	.537		

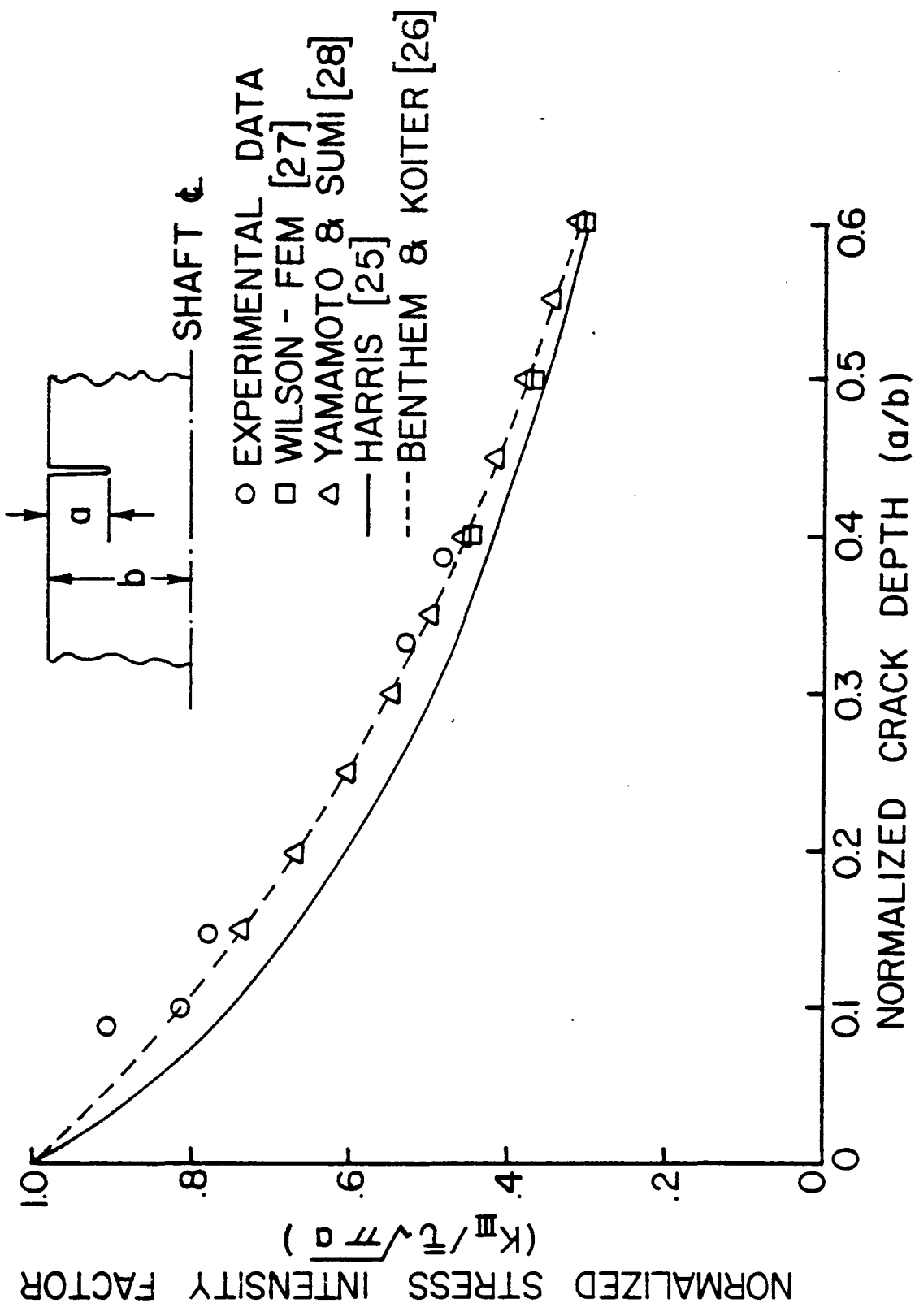

Figure 4.1 Comparison of Experimental Results with Analytical and Numerical Solutions

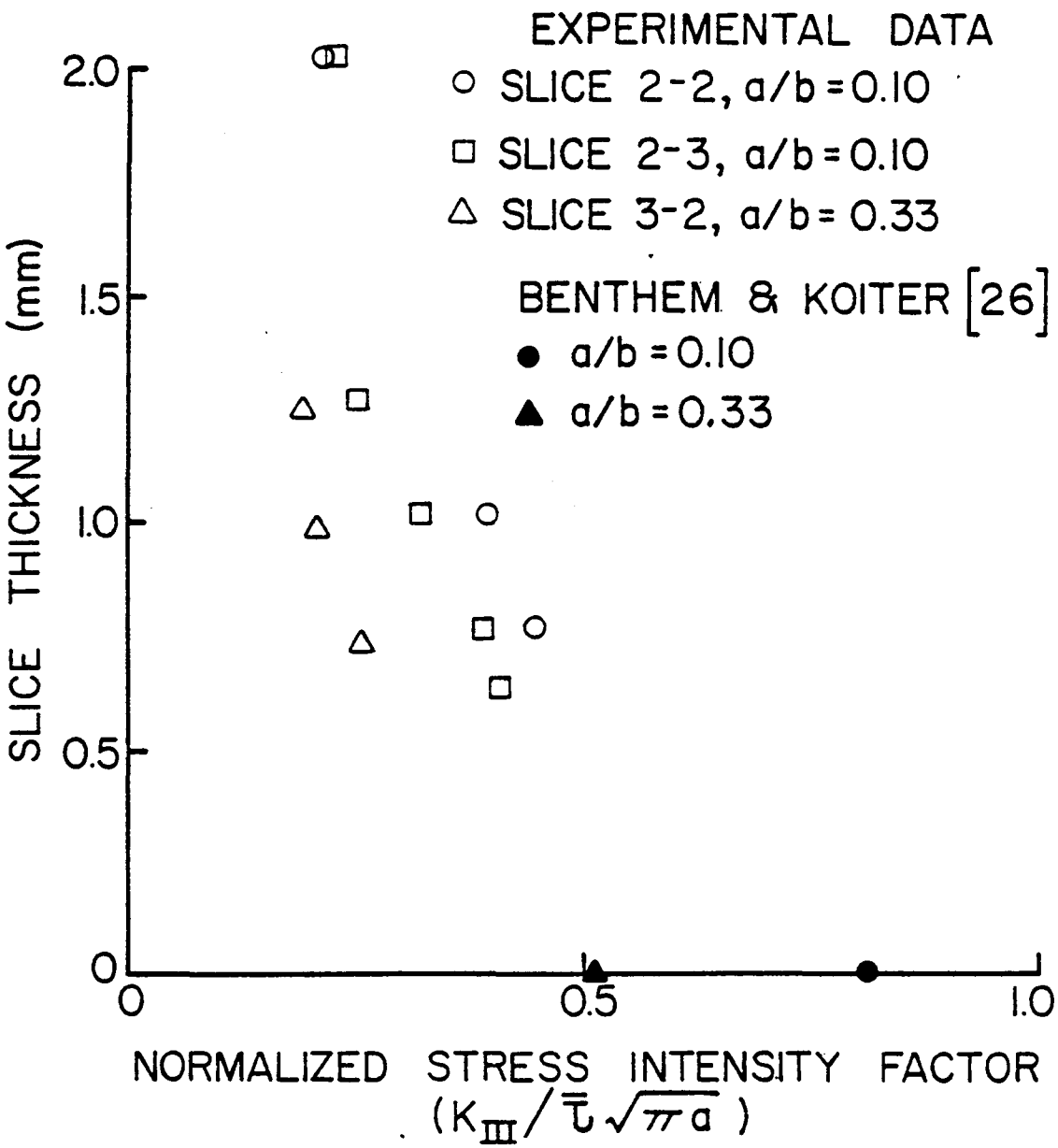

Figure 4.2 Experimental Results for Various Slice Thicknesses

It is obvious that the effects of slice thickness cannot be eliminated by using thin slices if the current slicing techniques are to be used. Therefore, modification in the method used to estimate stress intensity factors is necessary.

Slice thickness was found to have little or no effect on the results in previous work involving only Mode I or Mode II loadings. This is due to the fact that the slice taken to evaluate the stress intensity factors due to these loading conditions is cut in the n-z plane, i.e., perpendicular to the crack front. Since the stresses do not vary rapidly along the crack front, they can be considered to be nearly constant through the slice thickness. Thus, a slice can easily be made thin enough so that any through thickness variation of τ_{max} can be neglected and good results are obtained with little consideration for slice thickness effects.

If, on the other hand, the shear stress does vary through the slice thickness, the average value will differ from the value at the slice center unless the distribution happens to be exactly anti-symmetric with respect to the centerline. In a general case, the value of the shear stress at the center bears little relation to the average value. In particular, for pure Mode III loading, the shear stress τ_{zt} varies drastically through the thickness of the slice used in its determination, especially near the crack tip. Since measurements are made near the crack tip, it is evident that the results obtained may be in error if the thickness effects are not handled properly. Figure 4.3 shows the variation in the singular part of τ_{zt}, as given by Equation 2.1.

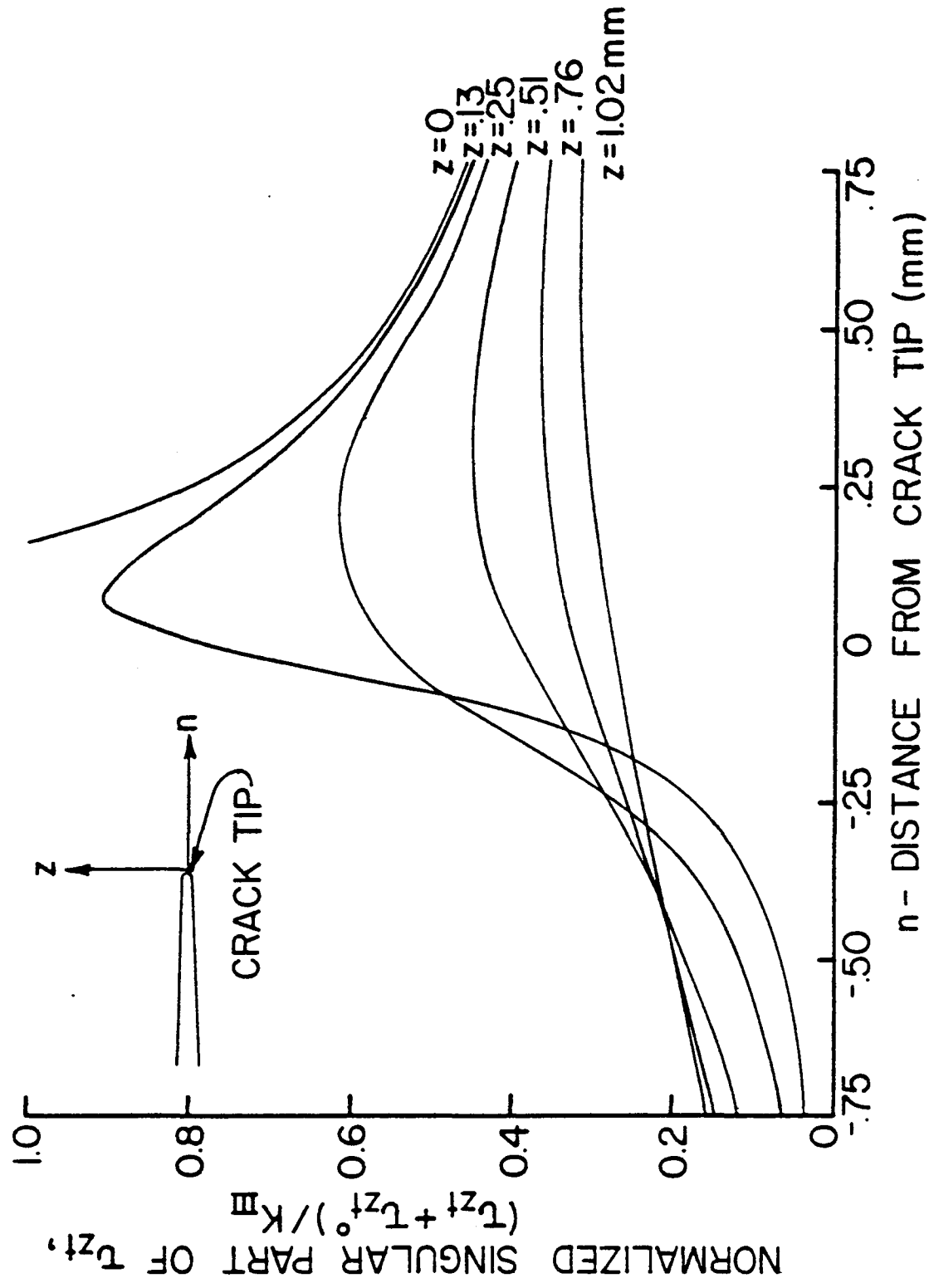

Figure 4.3 Variation of Shear Stress Through the Slice Thickness

The reason for the variation of shear stress for the case of Mode III loading is that both the distance from the crack tip (r) and the angle of rotation from the crack plane (θ) change along a line perpendicular to the slice surfaces. The value of shear stress measured at some point on a slice will be the average integrated through the thickness, of the values at the interior points along a line perpendicular to the plane of the slice and passing through the point at which the measurement is made. Hence, the value obtained will be dependent upon both the location relative to the crack tip and the slice thickness.

The stress intensity factor estimate is a function of the gradient of the shear stress as the crack tip is approached. It is observed that the average value of shear stress in a slice of non-zero thickness deviates from the value at the slice center. The deviation increases as the crack tip is approached and is greater in thicker slices (Figure 4.4). Therefore, the use of the average values of shear stress will result in an incorrect gradient and consequently an erroneous value of stress intensity factor. Figure 4.5 shows the effect of slice thickness on the singular part of the apparent stress intensity factor. It is easily seen that if straight lines are fitted to the regions of the curves between z = .25 mm and z = .75 mm (the region in which the experimentally determined linear zone is normally found) and extrapolated to z = 0 that the stress intensity factors thus estimated will be significantly lowered for increasing slice thicknesses, agreeing with the experimental results described previously.

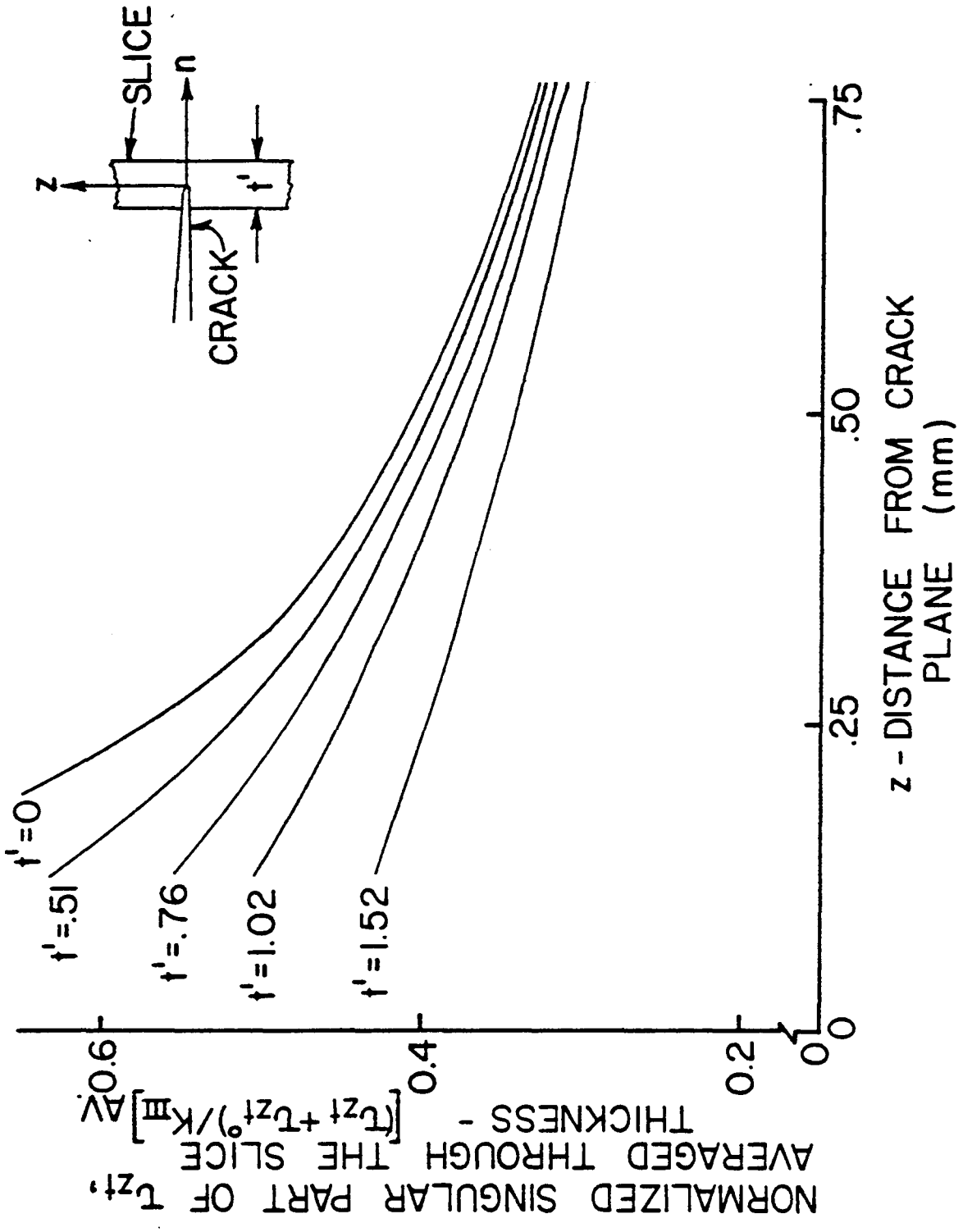

Figure 4.4 Variation of Average Shear Stress with Slice Thickness

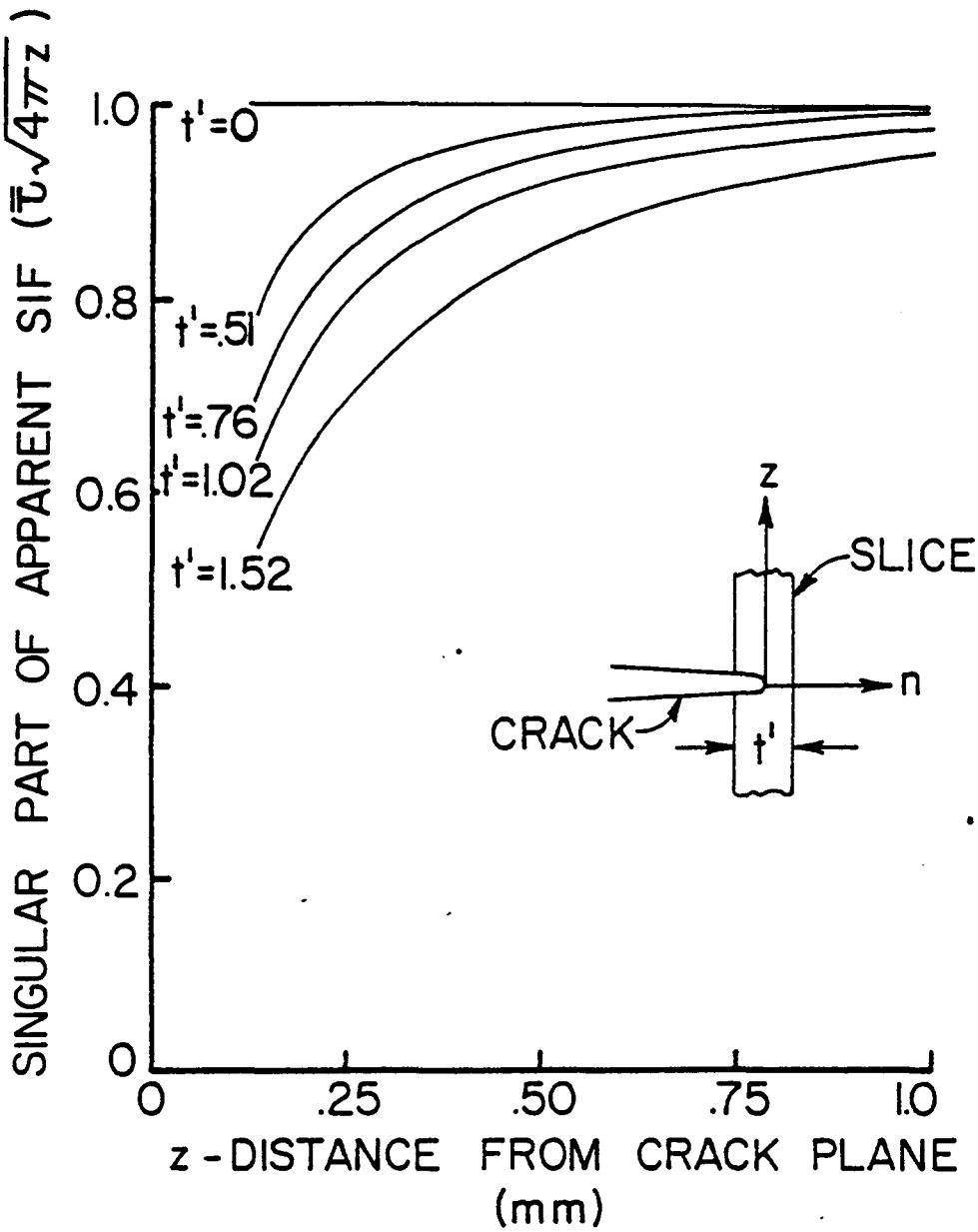

Figure 4.5 Variation of the Singular Part of Apparent Stress Intensity Factor with Slice Thickness

A method for estimating stress intensity factors using data obtained from single finite thickness slices with τ_{max} varying through the thickness is desired. The method will have to make use of an average value of shear stress. This average value can be used either directly, or as the basis for calculating the value in the $\theta = \frac{\pi}{2}$ plane. Using the average value directly is more appealing since it requires no assumptions about the distribution of stresses. This is the path chosen.

Intuitive reasoning leads to the conclusion that since the average shear stress is measured and used in the calculations for apparent stress intensity factor, the average radius from the crack tip should be used also. The average radius may be defined as:

$$\bar{r} = \frac{1}{t'} \int_{-t'/2}^{+t'/2} r \, dn \qquad (4.1)$$

where r is defined as $(n^2 + z^2)^{1/2}$ and the integral is taken holding z constant. When this value and the average value of shear stress are used to generate the family of curves on Figure 4.5, all curves are found to lie along the curve for t' = 0. The effect of slice thickness is thus eliminated.

Experimental verification was obtained by re-analyzing the data taken from the slices used previously in determining the effect of slice thickness on stress intensity factor estimates. In this case, all of the values obtained from a single slice were nearly identical, and thus, independent of slice thickness. This scheme is the one used to reduce all of the data presented in this thesis. However, it should be noted that this procedure may not be applicable if the slice

is not centered on the crack tip.

Inaccuracies in the stress intensity factor estimates are attributable to the difficulty in locating the slice with the notch tip at its center. The values of average radius calculated for a slice will be in error if the notch tip is not located properly. The error will be carried into the calculated values of K_{AP} and thence into the estimate of K_{III}.

Equations 2.1 indicate that K_{III} can be calculated either from the shear stress in the z-t plane as described previously or from the shear stress in the n-t plane. A closer analysis of these equations reveals that in only the z-t plane is the singularity approached in the plane of the slice required to evaluate the stress. A slice parallel to the n-t plane contains the plane $\theta = 0$; in this plane, the singular part of τ_{nt} will be zero. In order to evaluate τ_{nt}, a number of slices perpendicular to the line $\theta = \frac{\pi}{2}$ and at varying distances from the crack plane would have to be taken and τ_{nt} evaluated at this point in each slice. Then, if enough slices are taken, if the location of each slice is accurately determined, and if the point at which $\theta = \frac{\pi}{2}$ can be located accurately in each slice, τ_{nt} can be evaluated and K_{III} determined. The author attempted to use this procedure and found it to be both time consuming and very prone to error. For these reasons it was not used.

Several problems were encountered in the course of the test program which, while not directly contributing to errors, did make data more difficult to obtain. One problem was encountered in using machined notches rather than natural cracks. The slices from which

data were taken had to be thinner than the slices taken for Mode I data (approximately 1 mm thick rather than 2 mm) in order to obtain data close enough to the notch tip. This leads to fragile slices requiring careful handling, particularly during the sanding operation. Another problem concerned the curved front of the notch. This makes the location of the slice more difficult than would be the case if a straight front notch were used. The final problem involved the loading system used. The test specimens tended to crack around the loading pins, in some cases failure occurred. The cracking problem seems to be related to the existence of surface stresses in the specimen. Specimens with no or low surface stresses did not crack even under relatively high loads while those with higher surface stresses often cracked under much lower loads. Hole preparation did not seem to be a factor. In any case, the cracking is caused by high contact stresses where the loading pins meet the hole edges. It is advised that the loading system be altered before attempting to run further tests of this type. This could be done by the use of "soft" pins, i.e., silicone rubber coated. This will reduce the contact stresses by spreading the load over a larger area.

V. SUMMARY AND CONCLUSIONS

An experimental technique is described for obtaining data on the stress field in the vicinity of a crack tip from which the stress intensity factor arising from Mode III loading may be estimated. The method described was applied to a series of stress freezing photoelastic experiments involving circumferentially notched round bars loaded in torsion. The results obtained from these experiments are compared with analytical and numerical results drawn from the literature. The agreement is found to be quite good, with the experimental results generally being within five percent of the analytical.

It is concluded that the method described is a viable means for determining stress intensity factors for pure Mode III loadings. The extension to mixed mode problems will involve the inclusion of Mode I and Mode II effects. The techniques involved may prove useful in extracting data from slices having rapid stress variations through the thickness.

REFERENCES

1. Sneddon, I. N., "The Distribution of Stress in the Neighborhood of a Crack in an Elastic Solid", Proceedings of the Royal Society (London), Series A, Vol. 187, pp. 229-260, 1946.

2. Green, A. E. and I. N. Sneddon, "The Distribution of Stress in the Neighborhood of a Flat Elliptical Crack in an Elastic Solid", Proceedings of the Cambridge Philosophical Society, Vol. 46, pp. 159-163, 1950.

3. Shah, R. C. and A. S. Kobayashi, "Stress Intensity Factor for an Elliptical Crack Under Arbitrary Normal Loading", Journal of Engineering Fracture Mechanics, Vol. 3, No. 1, pp. 1971.

4. Swedlow, J. L., Ed., "The Surface Crack's Physical Problems and Computational Solutions", Symposium Proceedings, ASME Committee for Computing in Applied Mechanics of AMD, Nov. 1972.

5. Rybicki, E. F. and S. E. Benzley, Eds., "Computational Fracture Mechanics", Symposium Proceedings ASME Computer Technology Committee of Pressure Vessels Division, June 1975.

6. Irwin, G. R., Discussion, Proceedings of the Society for Experimental Stress Analysis, Vol. 16, No. 1, pp. 42-96, 1958.

7. Smith, D. G. and C. W. Smith, "A Photoelastic Evaluation of the Influence of Closure and Other Effects upon the Local Bending Stresses in Cracked Plates", International Journal of Fracture, Vol. 6, No. 3, pp. 305-318, September 1970.

8. Marrs, G. R. and C. W. Smith, "A Study of Local Stresses Near Surface Flaws in Bending Fields", Stress Analysis and Growth of Cracks, pp. 22-36, October 1972.

9. Smith, D. G. and C. W. Smith, "Photoelastic Determination of Mixed Mode Stress Intensity Factors", Engineering Fracture Mechanics, Vol. 4, No. 2, pp. 35-360, June 1972.

10. Schroedl, M. A., J. J. McGowan and C. W. Smith, "An Assessment of Factors Influencing Data Obtained by the Photoelastic Stress Freezing Technique for Stress Fields Near Crack Tips", Engineering Fracture Mechanics, Vol. 4, No. 4, pp. 801-809, December 1972.

11. Schroedl, M. A. and C. W. Smith, "Local Stresses Near Deep Surface Flaws Under Cylindrical Bending Fields", Progress in Flaw Growth and Fracture Toughness Testing, ASTM STP 536, pp. 49-63, October 1973.

12. Smith, C. W., "Use of Three Dimensional Photoelasticity in Fracture Mechanics", Experimental Mechanics, Vol. 13, No. 12, pp. 539-544, December 1973.

13. Schroedl, M. A. and C. W. Smith, "A Study of Near and Far Field Effects in Photoelastic Stress Intensity Determination", Engineering Fracture Mechanics, Vol. 7, No. , pp. 341-355, 1975.

14. McGowan, J. J. and C. W. Smith, "A Finite Deformation Analysis of the Near Field Surrounding the Tip of Crack-like Elliptical Perforations", International Journal of Fracture, Vol. 11, No. 6, pp. 977-987, December 1975.

15. Jolles, M., J. J. McGowan and C. W. Smith, "Use of a Hybrid Computer Assisted Photoelastic Technique for Stress Intensity Determination in Three-Dimensional Problems", Computational Fracture Mechanics, ASME-AMD-SP, pp. 83-102, June 1975.

16. Smith, C. W., J. J. McGowan and M. Jolles, "Effects of Artificial Cracks and Poisson's Ratio Upon Photoelastic Stress-Intensity Determination", Experimental Mechanics, Vol. 16, No. 5, pp. 188-193, May 1976.

17. Kobayashi, A. E., Ed., Experimental Fracture Mechanics II, Society for Experimental Stress Analysis Monograph No. 2, Chapter 1, pp. 3-58, Iowa State University Press, 1975.

18. Smith, C. W., M. Jolles and W. H. Peters, "Stress Intensities for Cracks Emanating from Pin-Loaded Holes", Flaw Growth and Fracture, ASTM STP 631, pp. 190-201, 1977.

19. Smith, C. W. and W. H. Peters, "Experimental Observations of 3D Geometry Effects in Cracked Bodies", Developments in Theoretical and Applied Mechanics, Vol. 9, pp. 225-234, May 1978.

20. Smith, C. W., A. T. Andonian and W. H. Peters, "Stress Intensity Distributions for Surface Flaws Under Mixed Mode Loading", (in Press), USAF FDL Report Contr. No. F33615-76-C03078, 1978.

21. Inglis, C. E., "Stresses in a Plate Due to the Presence of Cracks and Sharp Corners", Proceedings of the Institution of Naval Architects, 1913.

22. Griffith, A. A., "The Phenomena of Rupture and Flow in Solids", Phil. Trans. of the Royal Society (London), Series A, Vol. 221, pp. 163-198, 1920.

23. Irwin, G. R., "Analysis of Stresses and Strains Near the End of a Crack Traversing a Plate", Journal of Applied Mechanics, Vol. 24, No. 3, pp. 361-364, September 1957.

24. Kassir, M. K. and G. C. Sih, "Three-Dimensional Stress Distribution Around an Elliptical Crack Under Arbitrary Loadings", Journal of Applied Mechanics, Vol. 33, No. 3, pp. 601-611, September 1966.

25. Harris, D. O., "Stress Intensity Factors for Hollow Circumferentially Notched Round Bars", Journal of Basic Engineering, Vol. 89, No. 1, pp. 49-54, March 1967.

26. Benthem, J. P. and W. T. Koiter, "Asymptotic Approximations to Crack Problems", Methods of Analysis and Solutions of Crack Problems, G. C. Sih, Ed., Noordhoff, Holland, 1973.

27. Wilson, W. K., "On Combined Mode Fracture Mechanics", Research Report 69-1E7-FMECH-R1, Westinghouse Research Laboratories, 1969.

28. Yamamoto, Y. and Y. Sumi, "Stress Intensity Factors for Three-Dimensional Cracks", International Journal of Fracture, Vol. 14, No. 1, pp. 17-35, February 1978.

29. Gross, B. and A. Mendelson, "Plane Elastostatic Analysis of V-Notched Plates", International Journal of Fracture, Vol. 8, No. 3, pp. 267-276, September 1972.

30. Oppel, G., "The Photoelastic Investigation of Three-Dimensional Stress and Strain Conditions", National Advisory Committee for Aeronautics, Technical Memorandum No. 824, 1937.

31. Dally, J. W. and W. F. Riley, Experimental Stress Analysis, McGraw-Hill, 1965.

32. Frocht, M. M., Photoelasticity, John Wiley and Sons, 1948.

The vita has been removed from the scanned document

A PHOTOELASTIC TECHNIQUE FOR THE DETERMINATION OF STRESS INTENSITY FACTORS FOR MODE III LOADING

by

William Thor Hardrath

(ABSTRACT)

A method for extracting estimates of the stress intensity factors due to Mode III loadings from photoelastic data is developed. The results are supported by a series of stress freezing photoelastic experiments conducted on circumferentially notched round bars to which torsional loads were applied yielding a pure Mode III loading condition at the notch tip. Photoelastic data were taken from slices cut from the test specimens near the notch tip and stress intensity factors obtained. Results are compared with numerical and analytical results drawn from the literature.